Compositional dependence of the luminescence of $In_{0.49}(Al_yGa_{1-y})_{0.51}P$ alloys near the direct–indirect band-gap crossover

J. S. Nelson and E. D. Jones
Semiconductor Materials and Device Sciences Department, 1113, MS-0601, Sandia National Laboratories, Albuquerque, New Mexico 87185

S. M. Myers and D. M. Follstaedt
Semiconductor Nanostructure Physics Department, 1112, MS-1414, Sandia National Laboratories, Albuquerque, New Mexico 87185

H. P. Hjalmarson
Compound Semiconductor Technology Department, 1322, MS-0603, Sandia National Laboratories, Albuquerque, New Mexico 87185

J. E. Schirber
Solid State Sciences Department, 1100, MS-1437, Sandia National Laboratories, Albuquerque, New Mexico 87185

R. P. Schneider
Semiconductor Materials Department, 1311, MS-0603, Sandia National Laboratories, Albuquerque, New Mexico 87185

J. E. Fouquet, V. M. Robbins, and K. W. Carey
Hewlett Packard Laboratories, 3500 Deer Creek Road, Palo Alto, California 94303

(Received 2 November 1995)

A number of complementary experimental characterization tools and theoretical band structure methods were used to determine unambiguously the band-edge luminescence as a function of Al concentration, and to place an upper limit on the short-wavelength emission of InAlGaP alloys lattice matched to GaAs. In particular, the direct-to-indirect band-gap crossing has been determined by analyzing a series of metalorganic vapor-phase-epitaxy-grown $In_{0.49}(Al_yGa_{1-y})_{0.51}P$ alloys lattice matched to GaAs with double-crystal x-ray analysis, Rutherford backscattering spectroscopy, pressure- and temperature-dependent photoluminescence, and transmission electron microscopy. The experimental measurements are compared to first-principles plane-wave pseudopotential band structure calculations for the ternary end points, InGaP and InAlP. The maximum room temperature direct band gap is found to be 2.24 eV, corresponding to an Al composition of $y=0.52\pm0.02$, in good agreement with the theoretical prediction of 0.58 ± 0.05.

I. INTRODUCTION

The phosphide-based quaternary alloy $In_x(Al_yGa_{1-y})_{1-x}P$ lattice matched to GaAs is one of the most important material systems for visible photonic devices (lasers and light-emitting-diodes). The wavelength can be tuned from red to green by changing the Al to Ga mole fraction y. Unfortunately, as the Al concentration is increased, the radiative efficiency of InAlGaP alloys appears to decrease dramatically. For example, at $y=0.5$ the luminescence intensity is reduced by two orders of magnitude as compared to $y=0$. It has been suggested that this decrease is due to an increase in nonradiative defects or a direct to indirect crossing as the Al mole fraction is increased, or both. To distinguish between these two mechanisms, and to ultimately realize the full potential of InAlGaP alloys for photonic applications, a systematic study of the compositional dependence of the band-edge luminescence is required.

Many measurements of the compositional dependence of the band-edge luminescence of ordered and disordered alloys of $In_{0.5}(Al_yGa_{1-y})_{0.5}P$ have been made previously.[1–12] In general, the short-wavelength limit for detectable photoluminescence (PL) intensity occurs between 2.24–2.30 eV at room temperature (RT), with the luminescence intensity dropping two to three orders of magnitude from $y=0.0$ to $y=0.4-0.7$. The lower end of these values (2.24 eV) can often times be correlated with CuPt-type ordering.[13–15] Consistent with this observation, Gavrilovic *et al.*[13] found the band gap of InAlGaP increases with post-growth annealing or impurity diffusion; both of these procedures decreased the amount of ordering found in the sample. Hayakawa *et al.*[6] obtained RT PL at 2.30 eV for $y=0.65$ in Si-doped $In_{0.5}(Al_yGa_{1-y})_{0.5}P$. The intensity at this Al concentration was three orders of magnitude lower than at $y=0.0$. They did not characterize whether the PL was Γ-, X, or impurity-related. Nozaki *et al.*[5] obtained liquid helium (LH) PL from both the direct (Γ) and indirect band edges (X) up to $y=1.0$, and noted that different band edges could be distinguished by a change in slope (PL intensity versus alloy composition) at approximately $y=0.4$. The limiting wavelength found by Nozaki *et al.*[5] was 2.29 eV at 4.2 K for $y=1.0$ (InAlP). This is in contrast to the results of Hayakawa *et al.*,[6] which, when extrapolated to LH, would be 2.37 eV at $y=0.65$. Ohba *et al.*[3] found a limiting wavelength of 2.26 eV at 300 K for $y=0.53$; the PL energy increased linearly up to this point with no slope change, indicating a Γ-like band-

edge luminescence. Interestingly, Ikeda *et al.*[2] also observed LH PL at 2.37 eV in Se-doped $In_{0.5}(Al_yGa_{1-y})_{0.5}P$. In this case, the sample composition was not determined, although this energy corresponded to an Al/Al+Ga mole-fraction ratio of 0.8 in the vapor phase during growth. More recently, Mowbray *et al.*[11] and Prins *et al.*[12] reported direct-to-indirect crossovers in $In_{0.5}(Al_yGa_{1-y})_{0.5}P$ at $y=0.50$ and 0.58, with limiting wavelengths of 2.33 (4.2 K) and 2.25 eV (300 K), respectively.

The relative scatter in the published upper limit on the Al mole fraction at which PL can be obtained is primarily due to two factors: differences in sample growth techniques (ordered versus disordered, doping levels) and the lack of an independent structural characterization of the as-grown alloy. Without an independent structural analysis, the Al concentration is only indirectly inferred from either assumed band-gap variations, growth runs of binary and ternary alloys, or x-ray analysis. The use of x-ray analysis to determine composition is uncertain since GaP and AlP are nearly lattice matched. These factors have led to an uncertainty in the Al concentration at which the direct-to-indirect transition in $In_{0.5}(Al_yGa_{1-y})_{0.5}P$ occurs. To design efficient short-wavelength photonic devices from this material system, i.e., vertical-cavity-surface-emitting lasers (VCSEL's) and light-emitting diodes (LED's), an accurate representation of the quaternary band structure is essential.

In this paper, a number of complementary experimental characterization tools and theoretical band structure methods were used to determine unambiguously the band-edge luminescence as a function of Al mole fraction, and to place an upper limit on the short-wavelength emission of $In_{0.49}(Al_yGa_{1-y})_{0.51}P$ alloys lattice matched to GaAs, i.e., the direct-indirect (Γ-X) crossover. In particular, we have analyzed a series of metalorganic vapor phase epitaxy (MOVPE)-grown $In_{0.49}(Al_yGa_{1-y})_{0.51}P$ alloys lattice matched to GaAs with double-crystal x-ray (DCX) analysis.[16] Rutherford backscattering spectrometry (RBS),[17] pressure- and temperature-dependent PL,[18] and high-magnification, dark-field transmission electron microscopy (TEM).[19] The experimental measurements are compared to first-principles plane-wave pseudopotential band structure calculations[20] for the ternary end points, InGaP, and InAlP.

II. METHODS

A. Experimental methods

Two types of samples were prepared and studied in this work, epilayers and double heterostructures. The epilayers consisted of micrometer-thick $In_{0.49}(Al_yGa_{1-y})_{0.51}P$ alloys lattice matched to GaAs and the second type is a double heterostructure device consisting of a micrometer-thick $In_{0.49}(Al_yGa_{1-y})_{0.51}P$ layer sandwiched between two InAlP barriers on a GaAs substrate.

The epilayer samples were grown on a low pressure IR-lamp-heated MOVPE system with a horizontal quartz reaction chamber opening into a purged N_2-filled glove box. A growth pressure of 110 mbar was used, with a total flow rate of approximately 11 slm. The V/III ratio was ~150. Sources include adduct-purified trimethylindium and triethylgallium (Air Products), oxygen-reduced grade trimethylaluminum (Morton International), and pure phosphine (Phoenix). A

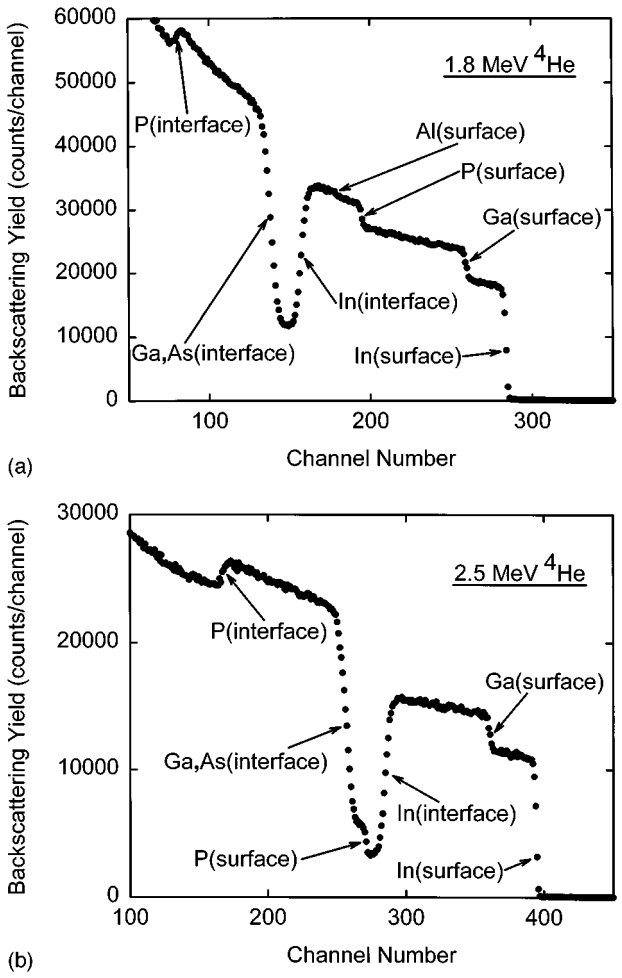

FIG. 1. A representative backscattering spectrum from an uncapped InAlGaP sample on GaAs obtained with 1.8 MeV (a) and 2.5 MeV (b) He. Several of the steps corresponding to the surface and substrate interface are labeled in the figure.

Millipore Waferpure phosphine purifier was used in-line. Four quarter-wafer GaAs pieces were loaded onto a graphite susceptor for each growth run. The substrates were all (100) GaAs, misoriented 2° towards [010] (nearest ⟨110⟩). All layers exhibited mirrorlike surfaces, and each growth run was confirmed lattice matched to GaAs within $\Delta a/a<5\times10^{-4}$ using DCX rocking curve measurements. All samples were grown at a temperature of 750 °C or higher to avoid ordering; this was confirmed by the TEM measurements discussed below.

Since AlP and GaP are nearly lattice matched (<0.2%), the DCX analysis only fixes the In concentration, assuming zero lattice parameter bowing of the quaternary. To obtain the Al/Al+Ga mole-fraction ratio, RBS analysis was performed. For the $In_{0.49}(Al_yGa_{1-y})_{0.51}P$ alloy RBS can accurately determine both the In/P and In/Ga mole fractions, from which the Al concentration can be deduced. For consistency, the In/P can be compared to the DCX results; for lattice-matched samples this ratio is found to be 0.50 ± 0.02. A representative backscattering spectrum from uncapped $In_{0.49}(Al_yGa_{1-y})_{0.51}P$ on GaAs, obtained with 1.8-MeV He, is shown in Fig. 1(a), where several of the steps corresponding to the surface and substrate interface are labeled. One channel on the horizontal axis corresponds to an energy in-

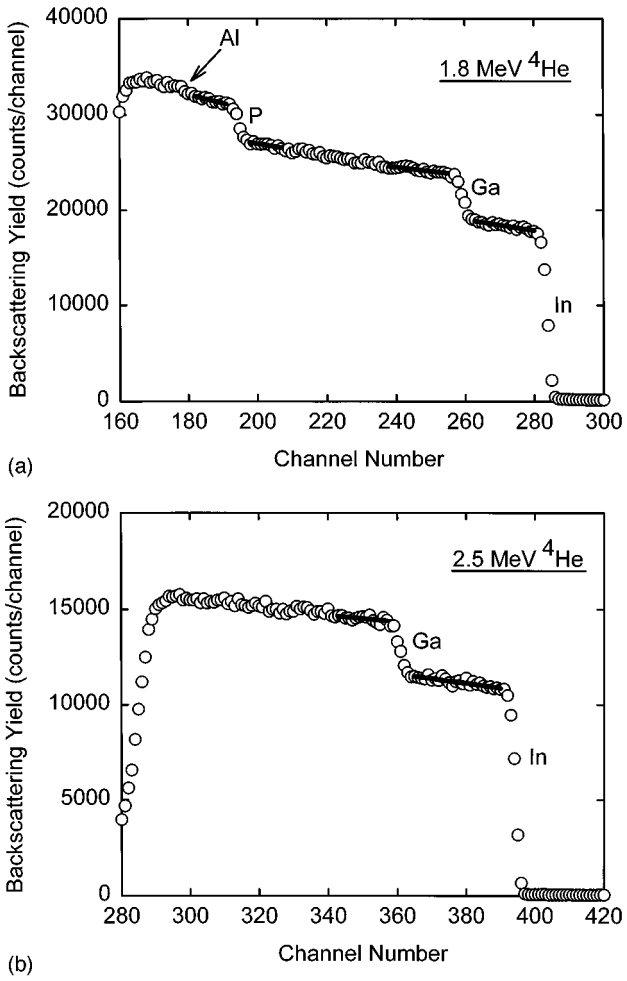

FIG. 2. Expanded backscattering spectrum of Fig. 1, together with least-squares-fit lines that were used to determine the step amplitudes. See text for more details of the analysis.

terval of 5.51 keV. Figure 1(b) shows a spectrum from the same sample obtained with 2.5-MeV He. At the higher energy the edges are more separated and the yields vary less with energy, but the number of counts per channel is less for the same beam charge, and the P surface step lies above other spectral structures, making quantitative analysis of this constituent difficult. Consequently, both analysis energies are useful in the case of uncapped specimens.

Figure 2 shows an expanded view of the spectrum in Fig. 1, together with least-squares-fitted lines that were used to determine the step amplitudes. For each step, the lines on either side were extrapolated to the middle of the step, and the difference between the extrapolated values was then taken as the step amplitude Y. Hence, the compositions reported later correspond to the upper portion of the films. The ratio of the concentrations of constituents [1] and [2] is given by

$$\frac{[1]}{[2]}=\left\{\frac{Y_1}{Y_2}\right\}\left\{\left(\frac{d\sigma}{d\Omega}\right)_2\Big/\left(\frac{d\sigma}{d\Omega}\right)_1\right\}\left\{\frac{S_1}{S_2}\right\}, \qquad (1)$$

with

$$S_z=K_z|\sec\theta_{\rm in}|\varepsilon(E_0)+|\sec\theta_{\rm out}|\varepsilon(K_zE_0). \qquad (2)$$

Here $(d\sigma/d\Omega)_z$ is the differential cross section for elastic backscattering from the nucleus of a Z atom, K_z is the fraction of the energy of the He ion that is retained after the nuclear scattering event, $\varepsilon(E)$ is the energy-dependent average energy-loss cross section per atom in the film, E_0 is the energy of the incident He beam, and $\theta_{\rm in}$ and $\theta_{\rm out}$ are the angles between the sample normal and, respectively, the incoming beam and the outgoing backscattered particles that enter the detector. The nuclear cross section $(d\sigma/d\Omega)_z$ is known very accurately, being nearly proportional to Z^2 in the center-of-mass frame with a well characterized correction of $\sim$1% due to electron screening.[17] The backscattering energy factor K_z is also accurately known. The electronic-stopping cross section ε is obtained by linearly combining experimentally determined cross sections for the elemental constituents.[17] As a result, the quantity S_z may be in error by as much as 10%. Fortunately, however, S_z varies smoothly with Z, and the derivative is known to about the same fractional accuracy as the magnitude. Consequently, since the value of S_z changes by only $\sim$2% from In to Ga and by $\sim$10% from In to P, the ratios of this parameter appearing in Eqs. (1) and (2) are judged to have inconsequential uncertainties.

Axial and planar ion channeling are of concern for accurate concentration measurements in single-crystal materials. Equations (1) and (2) are based on the absence of randomization of such effects. To avoid channeling, the sample normal was tilted 5° from the incident He beam and continuously rotated about its normal during the measurement. The solid-state detector was positioned at a scattering angle of 170° and at 15° from the sample normal. The need for this unusually elaborate procedure was illustrated by a spectrum obtained when one of the samples was tilted, but not rotated. The effect on the spectrum was quite noticeable, presumably due to the accidental coincidence of the beam or detector with some unidentified crystalline plane in the sample.

Temperature- and pressure-dependent PL were used to determine the band-gap variation with Al/Al+Ga mole-fraction ratio. The pressure dependence was found to be extremely useful for two reasons. First, since the Γ and X band gaps have opposite pressure derivatives (positive for Γ and negative for X), unambiguous state determination could be made. For all the samples reported here, the reported PL was Γ-like, with all positive pressure derivatives. Once the energy of the Γ state was larger than the X state, either by applying pressure or changing the Al composition, no PL could be observed. The second useful effect of pressure is that the change in intensity with pressure could be mapped on to the change in intensity with composition, i.e., pressure is ''equivalent'' to an increase in Al concentration. Thus we could follow several samples through the direct-to-indirect transition with both pressure and composition. Since the intensities for pressure and composition followed similar curves (see below) this indicated that most of the intensity decrease in $In_{0.49}(Al_yGa_{1-y})_{0.51}P$ is more likely due to non-Al-related defects. InGaP under pressure exhibited a similar intensity decrease as Al was added.

The experimental configuration for the PL measurements is described in Refs. 21 and 22. However, a brief description will be given here. The argon-ion laser power is coupled into a glass optical fiber (core diameter=100 μm) by means of a

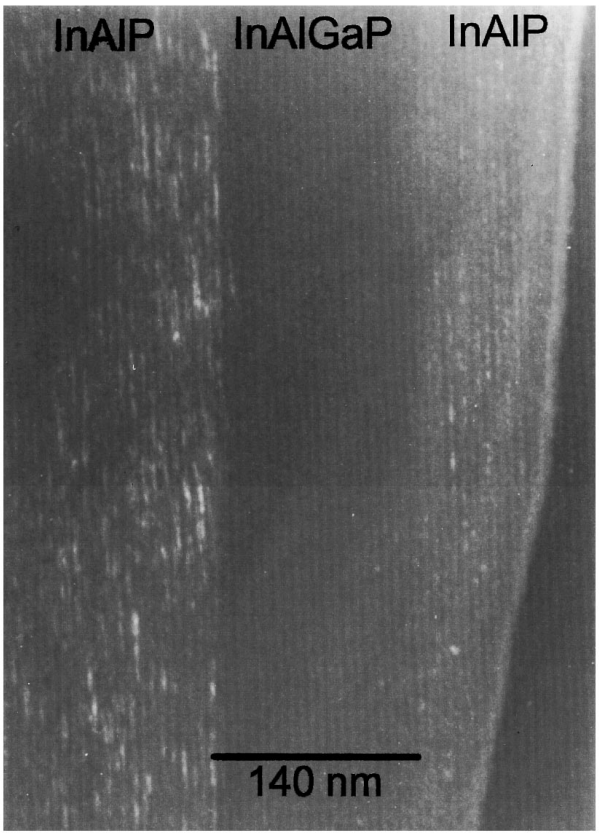

FIG. 3. Transmission electron microscopy dark-field image of InAlP/InAlGaP/InAlP heterostructure. Ordered domains (white linear features) are clearly seen in the lower barrier InAlP layer, and end abruptly at the InAlGaP active layer.

beam splitter and a microscope objective. The same fiber is used to transmit the laser light to the sample and to return the luminescence signal, which is directed to the monochromator and the data acquisition system. Laser power densities at the sample were of the order of 1 W/cm^2 and PL studies were made at temperatures of 4.0 (liquid helium), 76.0 (liquid nitrogen), and 300 K (RT). The hydrostatic-pressure-dependent PL measurements were made using a high-pressure helium gas system. The sample is attached to the polished end of the optical fiber by means of GE7031 varnish, thinned with a 50/50 mixture of toluene and methanol. The pressure chamber size (0.32-cm inside diameter) limits the sample size. Typical sample sizes are 0.16 cm square. Pressure is applied to the sample by high-pressure helium gas before the probe is inserted into the low-temperature bath in order to insure against pressure leaks. By limiting the lowest temperatures to liquid nitrogen (76 K), the helium pressure media remains in the gas phase, thereby allowing pressure changes at these temperatures without a warming cycle.

Several alloys of $In_{0.5}Ga_{0.5}P$ grown at various temperatures[10] and an $In_{0.49}(Al_{0.44}Ga_{0.56})_{0.51}P$ alloy between $In_{0.5}Al_{0.5}P$ barrier layers (double heterostructure) were examined with TEM using electron diffraction and dark-field imaging. The $In_{0.5}Al_{0.5}P$ alloys grown between 600 and 725 °C showed CuPt-type ordering; it was strongest at 675 °C, but could be eliminated by growing at 750 °C or higher.[19] When the double heterostructure was examined with electron diffraction, CuPt ordering reflections were observed. Dark-field imaging with a $\{111\}_B$ ordering reflection was then used to determine which layers were ordered, as shown in Fig. 3. With this technique, the ordered domains are illustrated. A relatively small 5-μm objective aperture was used in our instrument (Philips CM20T; objective focal length 2.7 mm; 0.27-nm resolution achievable) to maximize the contrast due to ordering and minimize interference from the zinc-blende reflections, albeit at the cost of image intensity. Ordered domains are readily found in the lower $In_{0.5}Al_{0.5}P$ barrier layer and less domains are seen in the upper layer, but domains are not detected in the 140-nm thick $In_{0.49}(Al_{0.44}Ga_{0.56})_{0.51}P$ alloy layer, as seen in Fig. 3. Their shape indicates that they are platelets being viewed edge on, ~3 nm thick and 30–80 nm across; similar ordered domains were seen in $In_{0.5}Ga_{0.5}P$.[19]

The detection of domains in layers on both sides of the $In_{0.49}(Al_{0.44}Ga_{0.56})_{0.51}P$ alloy layer clearly shows that if a similar degree of ordering were present in this alloy, it would have been detected. The less intense order in the upper layer may be due to the specimen's being thinner at this position. The ordered reflections from the $In_{0.5}Al_{0.5}P$ barrier layers are relatively weak compared to those for well ordered $In_{0.5}Ga_{0.5}P$; they are similar to reflections detected with weakly ordered $In_{0.5}Ga_{0.5}P$ where the band gap was reduced by only ~20 meV (grown at 600 °C) or ~40 meV (725 °C).[19] We infer that any undetected order present in the $In_{0.49}(Al_{0.44}Ga_{0.56})_{0.51}P$ alloy probably results in a band-gap reduction less than ~40 meV.

B. Theoretical methods

The electronic and optical properties of disordered InAlP alloys were modeled using the special-quasirandom structures (SQS) proposed by Wei *et al.*[23] The quaternary alloy is decomposed into ternary end points, InGaP and InAlP, with each ternary alloy treated at different levels of sophistication, i.e., virtual-crystal approximation (VCA), SQS-2, and SQS-4. The electronic properties were calculated within the local-density approximation[24] (LDA) of density functional theory,[25] using the generalized norm-conserving pseudopotentials of Hamann,[26] the exchange-correlation potential of Ceperly-Alder,[24] and a highly converged plane-wave expansion. The nonlinear core charge correction (NLCCC) of Louie and Froyen[27] was used consistently for Al, Ga, In, and P, although it makes very little difference for Al and P. The Brillouin sampling of the bulk structures were performed with 10 special k points,[28] and the SQS's with equivalent k-point sets proposed by Froyen.[29] A plane-wave energy cutoff of 24 Ry (used in all the calculations presented below) is sufficient for convergence of band gaps and valence bandwidths to less than 0.01 eV; the lattice parameters converge at a smaller value.

A kinetic model for the PL was used to predict the PL intensity from the computed band structure. The PL intensity depends on the ratio of radiative to nonradiative recombination rates. The nonradiative rate is dominated by defects of unknown origin. In this model, the concentration and electronic properties of the defect are assumed to be independent of alloy composition. This simple model is *post priori* justified by the surprisingly good agreement with the experimental data to be discussed below.

The key ingredient in the kinetic model is the composition and pressure dependence of the direct-to-indirect crossover. The PL intensity is determined by the fraction of carriers residing at the Γ point. These carriers are allowed to transfer between the Γ and X points via disorder or phonon scattering. The transfer rate is fast compared with the radiative rate. In fact, because the transfer rate is fast, the PL intensity becomes independent of this rate.

Because of the simple assumptions relating to the nature of the defects, it is assumed the nonradiative recombination rate is constant whether the carriers reside at the Γ or the X point.

The kinetic equations are

$$\frac{dn_\Gamma}{dt}=g_\Gamma-T_{\Gamma X}n_\Gamma+T_{X\Gamma}n_X-R_\Gamma n_\Gamma-r_\Gamma n_\Gamma, \tag{3}$$

$$\frac{dn_X}{dt}=g_X+T_{\Gamma X}n_\Gamma-T_{X\Gamma}n_X-R_X n_X-r_X n_X. \tag{4}$$

In Eqs. (3) and (4), the pump rates are g, the radiative rates are r, the nonradiative rates are R, and the transfer rates are T. For Eqs. (3) and (4) to be valid, the samples are assumed to be lightly doped, and the injected carrier density does not exceed the background majority carrier density. If this assumption is violated, bimolecular carrier kinetics would need to be assumed.

To compare with the steady state PL experiments, the time derivatives are set to zero. To a good approximation, it can be assumed that $g_X=0$. Adding Eqs. (3) and (4),

$$g_\Gamma=R_\Gamma n_\Gamma+r_\Gamma n_\Gamma+R_X n_X+r_X n_X. \tag{5}$$

This is a conservation rule for the total injected carrier density. Assembling,

$$n_X=\frac{T_{\Gamma X}n_\Gamma}{T_{X\Gamma}+R_X+r_X} \tag{6}$$

and

$$n_\Gamma=\frac{g_\Gamma}{R_\Gamma+r_\Gamma+[T_{\Gamma X}/(T_{X\Gamma}+R_X+r_X)](R_X+r_X)}. \tag{7}$$

The transfer rates are strongly temperature dependent and related by detailed balance. The rates can be written in terms of

$$f(T)=\exp(-\Delta_{X\Gamma}/k_BT), \tag{8}$$

where $\Delta_{X\Gamma}=|E_X-E_\Gamma|$ and T is the lattice temperature. The rates can be approximated as

$$T_{\Gamma X}=T_0N_Xf(T), \tag{9}$$

$$T_{X\Gamma}=T_0N_\Gamma \tag{10}$$

for the case $E_X>E_\Gamma$, and

$$T_{\Gamma X}=T_0N_X, \tag{11}$$

$$T_{X\Gamma}=T_0N_\Gamma f(T) \tag{12}$$

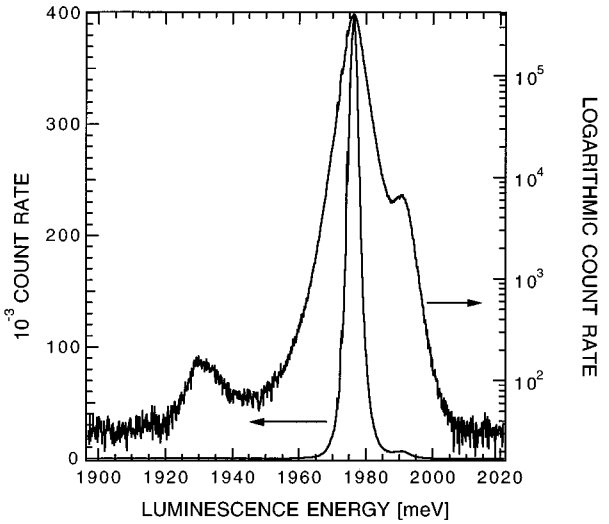

FIG. 4. Linear and logarithmic plots for an epilayer $In_{0.49}Ga_{0.51}P$ photoluminescence spectrum at 4.2 K. The small peak near 1930 meV is the 47-meV LO-phonon sideband and the small PL peak near 1990 is probably due to another disordered phase as described by Delong *et al.* (Ref. 30).

for the case $E_X<E_\Gamma$. These rates are written in terms of the elemental rate T_0 and the thermal density of states N_Γ and N_X.

The case in which the Γ point lies below the X point is of greatest practical interest. To a good approximation, the radiative rate from the X point can be ignored. Thus we set $r_x=0$. For this case, the luminescence intensity $I=r_\Gamma n_\Gamma$ can be written as

$$I=\frac{r_\Gamma g_\Gamma}{R_\Gamma+r_\Gamma+[T_0N_Xf(T)/(T_0N_\Gamma+R_X)]R_X}. \tag{13}$$

Furthermore, this expression simplifies to

$$I=\frac{r_\Gamma g_\Gamma}{R_\Gamma+r_\Gamma+[N_Xf(T)/N_\Gamma]R_X}, \tag{14}$$

using the fact that $T_0\gg R_X$.

Because the defects are assumed composition independent, $R=R_\Gamma=R_X$. Then

$$I=\frac{r_\Gamma g_\Gamma}{r_\Gamma+\{1+(N_x/N_\Gamma)f(T)\}R}. \tag{15}$$

III. RESULTS

A. Experimental results

The 4-K PL spectrum for a disordered $In_{0.49}Ga_{0.51}P$ epilayer sample is shown in Fig. 4. The full-width-at-half-maximum (FWHM) linewidth is about 4.5 meV, indicative of the good quality of these samples. In this paper, the peak energy of the PL spectrum is used as a measure of the bandgap energy of the sample. There are two extra peaks at 1930 and 1900 meV, indicated in the logarithmic PL plot in Fig. 4. The one near 1930 meV is the phonon sideband from the 47-meV LO phonon. The higher energy peak near 1990 meV is probably due to a portion of the sample which is ''more disordered'' as discussed recently by DeLong *et al.*,[30] who

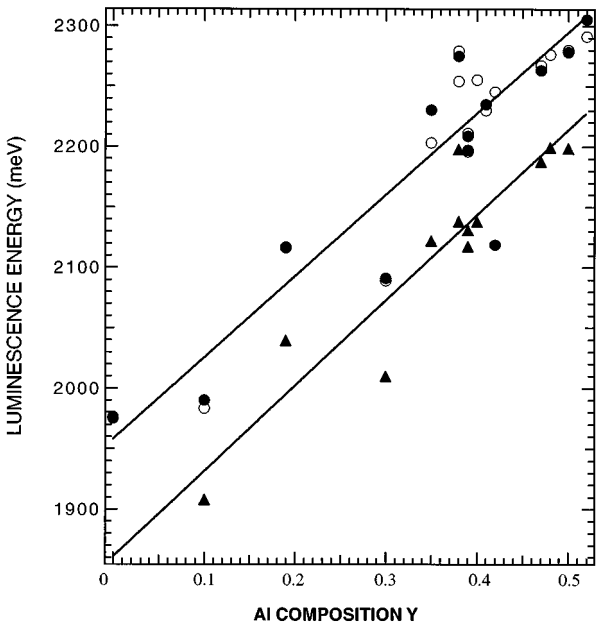

FIG. 5. Band-gap energies versus y at temperatures of 4 K (solid circles) and 76 K (open circles) and 300 K (solid triangles). The slopes are 629, 673, and 706 meV/Al, for 4, 76, and 300 K, respectively. For the sake of clarity, the 4-K least-squares fit is not drawn.

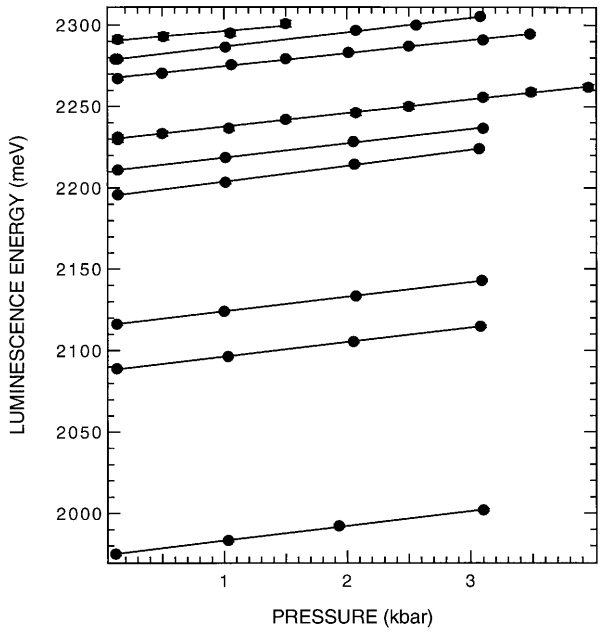

FIG. 6. Band-gap energy as a function of pressure at 76 K of $In_{0.49}(Al_yGa_{1-y})_{0.51}P$, for $y=0.2-0.5$. The straight lines drawn through the data have slope of 9.1 ± 0.3 meV/kbar.

conjectured that the ''true'' low-temperature band-gap energies of $In_{0.49}Ga_{0.51}P$ at 4 and 300 K are, respectively, 2011 and 1905 meV.

In order to study the Γ-X crossing, the band-gap energy was measured for a series of $In_{0.49}(Al_yGa_{1-y})_{0.51}P$ epilayers and double heterostructures, with Al concentrations ranging up to $y=0.52$. For concentrations greater than $y=0.52$, the PL signal was not observable, indicating that the Γ-point energy is higher than the X-point energy where nonradiative processes are thought to dominate. Figure 5 shows the PL-determined band-gap energies versus Al mole fraction for 4, 76, and 300 K. As outlined previously, the Al mole fractions were determined by RBS. A few samples were not characterized by RBS, therefore, the Al mole fractions of these samples were obtained from growth calibrations. The straight lines drawn through the data are a result of least-squares fit and are well described by the following linear equations:

$$\mathrm{Eg}(4\ \mathrm{K})=1962+629y \quad \mathrm{meV/Al},$$

$$\mathrm{Eg}(76\ \mathrm{K})=1958+673y \quad \mathrm{meV/Al},$$

and

$$\mathrm{Eg}(300\ \mathrm{K})=1861+706y \quad \mathrm{meV/Al}. \tag{16}$$

A lack of PL above 2.30 eV (or Al mole fraction of $y=0.52$) does not, by itself, unambiguously determine the direct to indirect band-gap cross over. By applying hydrostatic pressure to a series of samples with varying Al composition, direct band-gap samples could be followed through the direct-to-indirect band-gap crossing.

Figure 6 shows the 4-K band-gap variation with hydrostatic pressure for $In_{0.49}(Al_yGa_{1-y})_{0.51}P$, with Al mole fractions ranging from $y=0.2$ to 0.50. Independent of y, the alloys exhibit a positive pressure derivative of 9.1 ± 0.3 meV/kbar, indicating direct zone-center Γ transitions. A positive pressure derivative of this magnitude, distinguishes it from zone-edge X or L transitions with typical pressure derivatives of approximately -2.0 and $+2.0$ meV/kbar, respectively. Consistent with the temperature dependence, no PL could be obtained for pressures inducing band gaps above 2.30 eV.

The most obvious result attributed to the Γ-X crossing is a reduction in the peak intensity as the energy difference between the Γ and X conduction-band energies decreases. The decreasing PL intensity variation with composition is shown in Fig. 7. It is apparent that near Al mole fractions of about 50% (i.e., 76-K band-gap energies of about 2.30 eV), the intensity is dramatically reduced. The pressure dependence of the PL for a given Al concentration follows a similar trend; the intensity depends weakly on pressure and composition below $y=0.45$ and strongly near the direct to indirect crossing $y=0.52$.

B. Theoretical results

In this section, a direct comparison is made between the steady-state predictions of the kinetic theory with the PL data. The rates are chosen as follows: $r_r=10^9\ \mathrm{s}^{-1}$ and $r_x=0$ for the radiative rates, $R_\Gamma=R_X$ and $R_X=10^9\ \mathrm{s}^{-1}$ for the nonradiative rates. For the transfer rate, we take a value of $T_0=10^{-5}\ \mathrm{s}^{-1}\ \mathrm{cm}^3$. Using this value yields transfer time of approximately 10^{-12} s. Most direct gap semiconductors have rates similar to these values.

Figure 7 compares the experimental intensity at 76 K with the calculated efficiency $\varepsilon=I/g_\Gamma$ as a function of Γ-X energy difference (thermal densities of states are set equal to one and $T_0=10^{12}$). The excellent fit with experiment strongly supports the crossover occurring at Al mole fraction of 0.52, and the presence of a nonradiative recombination center.

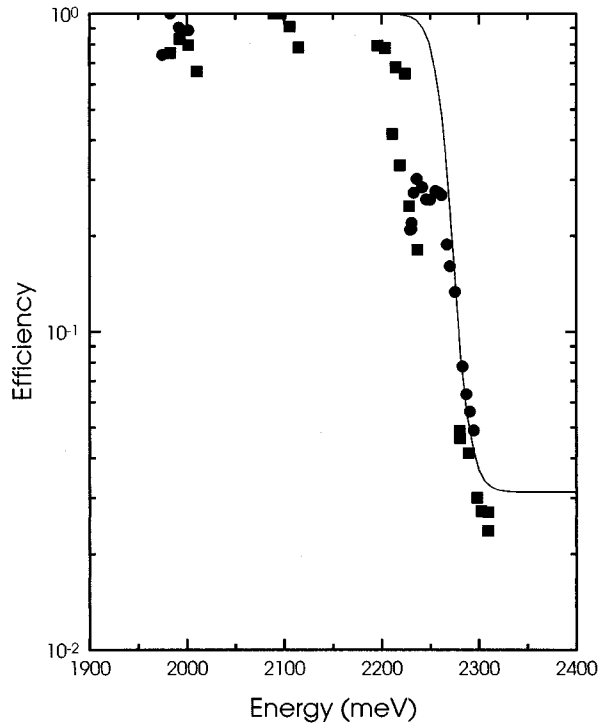

FIG. 7. Normalized 76-K photoluminescence intensity versus energy. The solid circles and squares are the epilayers and the double heterostructures. The solid line is the theoretical prediction of the intensity versus energy for 76 K.

The temperature- and pressure-dependent PL measurements do not provide information on the relative variation of the Γ, X, and L band-gap energies of $In_{0.49}(Al_yGa_{1-y})_{0.51}P$ with Al mole fraction. To obtain this information, first-principles plane-wave pseudopotential calculations were performed. As a guide to understanding the electronic states of $In_{0.5}(Al_yGa_{1-y})_{0.5}P$, a summary is given here of the calculated structural and electronic properties of bulk AlP, GaP, and InP. These results will also provide a way to test the sensitivity of the results for the direct-indirect crossing to the calculational details. For example, the LDA severely underestimates the absolute value of band-gap energies, whereas the band dispersions, i.e., Γ-X energy differences, are known to be in better agreement with experiment.

The calculated AlP, GaP, and InP lattice constants are 5.422, 5.356, and 5.834 Å, respectively. Typical of highly converged LDA calculations, the AlP and InP lattice constants are about 1% smaller than the experimental values of 5.46 and 5.87 Å. In the case of AlP, the NLCCC makes very little difference in the lattice parameter, ~0.01 Å, as expected. This is not the case for GaP and InP. Without the NLCCC (Ref. 27) the GaP lattice parameter is smaller than the experimental value of 5.45 Å by 3.2%, and with the NLCCC (Ref. 27) the lattice parameter is improved by 0.09 Å or 1.7% smaller than experiment. Although the calculated structural properties of GaP have been improved with the NLCCC, these results do not represent typical errors in well converged LDA calculations. This points to the importance of including the low-lying d-''core'' states in the calculation, to achieve 1% accuracy. The importance of d states in describing the structural and electronic properties of Ga- and In-based semiconductors has been discussed previously by Wright and Nelson.[31]

TABLE I. The zone-edge (Γ, X, and L) band gaps (eV) at the theoretical lattice parameters of AlP (5.422 Å), GaP (5.356 Å), and InP (5.834 Å), not including spin-orbit interactions. The experimental values are taken from Ref. 32. $\Delta(\Gamma$-$X)$ is the difference in energy of the direct band gap (Γ) and the indirect band gap (X). The value of the $\Delta(\Gamma$-$X)$ for AlP in parentheses is a theoretical value obtained from quasiparticle calculations of Ref. 33. The LDA correction is the difference between the experimental and theoretical band gaps.

	Eg(Γ)	Eg(X)	Eg(L)	$\Delta(\Gamma$-X): theory	$\Delta(\Gamma$-$X)$: expt.	LDA correction
AlP	3.26	1.42	2.74	1.84	1.12(1.87)	1.09
GaP	2.15	1.45	1.75	0.70	0.55	0.90
InP	0.59	1.61	1.37	−1.02	−0.96	0.87

The zone-edge (Γ, X, and L) band-gap energies at the theoretical lattice parameters of AlP, GaP, and InP are summarized in Table I. AlP and GaP exhibit indirect band gaps at the X point and InP has a direct band gap at Γ, consistent with experiment. The LDA band gaps are underestimated by ~50% of the experimental value. A more relevant quantity for the purposes here is the difference in energy of the Γ- and X-point conduction-band energies. These values are also reported in Table I. The LDA Γ-X conduction-band energy differences [$\Delta(\Gamma$-$X)$] of 1.84 (AlP), 0.70 (GaP), and 1.02 eV (InP) are in good agreement with the experiment values[32] of 0.55 (GaP) and 0.96 eV (InP). The experimental[32] Γ-X splitting of AlP is 1.12 eV, in contrast to theoretical estimates of 1.87 eV, based on the quasiparticle calculations of Xu and Louie.[33] Our results are consistent with the quasiparticle calculations. The LDA correction in Table I is the dif-

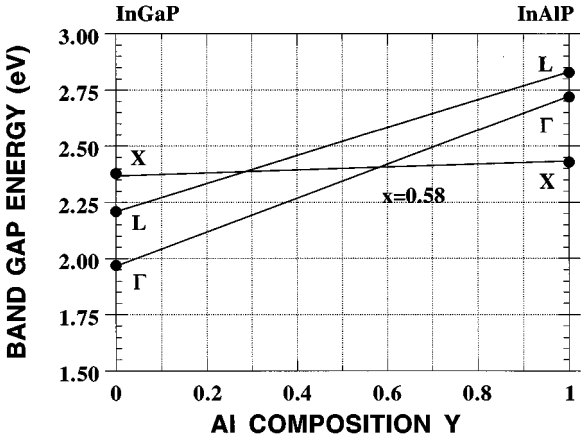

FIG. 8. Band-edge energies for the ternary endpoints $In_xGa_{1-x}P$ and $In_xAl_{1-x}P$, calculated with the plane-wave pseudopotential method using the SQS-4 representation of the ternary alloys (see text for more details). The band-edge states are assumed to vary linearly with composition between the two end points, i.e., obeying Vegard's law for quaternary alloys. The band-edge energies have been rigidly shifted to take into account local-density approximation errors and to make a more realistic comparison with measured values (see text for more details).

ference between the experimental and theoretical band gap energies; these values are within 0.2 eV for AlP, GaP, and InP, being the greatest for the larger band gap AlP. The discrepancy of ± 0.10 eV between the experimental and theoretical values of the Γ-X energy difference and the ± 0.2 eV difference in the LDA corrections to the band gaps places a limit on the accuracy of the prediction of the direct to indirect crossing of about $\pm 5\%$.

The direct-to-indirect crossing in $In_{0.49}(Al_yGa_{1-y})_{0.51}P$ is modeled using the SQS structures developed for disordered ternary III-V zinc-blende alloys. A comprehensive discussion of the SQS structures can be found in Ref. 23. For the purposes here, the calculations were performed using the SQS-4 representation of the ternary alloy end points, $In_{0.5}Ga_{0.5}P$ and $In_{0.5}Al_{0.5}P$. The SQS-4 structures are ordered $(InP)_2$-$(GaP)_2$ or $(InP)_2$-$(AlP)_2$ [110] superlattices. The Γ, X, and L band-gap energies are assumed to vary linearly between the ternary alloy end points. This approach was chosen rather than a virtual crystal approximation (VCA) of the group-III pseudopotentials, since the VCA does not accurately represent the true band gaps of disordered alloys containing local charge transfer and bond length and bond angle relaxations. The lattice parameters for the SQS-4 structures are chosen to obey Vegard's law and the internal coordinates are fully relaxed in the calculations.

Figure 8 shows the variation of the Γ, X, and L-band gap energies from $In_{0.5}Ga_{0.5}P$ to $In_{0.5}Al_{0.5}P$. The calculations predict the direct to indirect crossing to occur at an Al mole fraction of 0.58, $In_{0.5}(Al_{0.58}Ga_{0.42})_{0.5}P$, in reasonable agreement with the experimental value of 0.52, given the 0.1-eV uncertainties in the Γ-X energy separations of the binaries. The flat dispersion of the X point is related to its atomic character—the X-point conduction-band state is predominantly associated with the P anion. The slope of the Γ band gap is 0.75 eV/Al compared to the experimental value of 0.63 eV/Al (at 4 K).

IV. SUMMARY

Complementary experimental and theoretical techniques have been used to determine the compositional dependence of the luminescence of $In_{0.49}(Al_yGa_{1-y})_{0.51}P$ alloys near the direct-indirect band-gap crossover. The crossover occurs at an Al mole fraction of $y=0.52$, corresponding to a room-temperature band gap of 2.24 eV. A simple theoretical model based on a nonradiative recombination center accurately represents the essential features of the decrease in PL intensity as the crossover is approached. Since the PL intensity showed a similar variation with both pressure and Al composition, this suggests that the nonradiative recombination center is not *a priori* related to an increase in Al composition in the quaternary alloy, although this is certainly possible. To improve the short wavelength (>2.20 eV) optical properties of $In_{0.49}(Al_yGa_{1-y})_{0.51}P$, further study into the nature of the nonradiative centers in this material system is warranted.

[1] J. P. Andre, E. Dupont-Nivet, D. Moroni, J. N. Patillon, M. Erman, and T. Ngo, J. Cryst. Growth **77**, 354 (1986).

[2] M. Ikeda, K. Nakano, Y. Mori, K. Kaneko, and N. Watanabe, J. Cryst. Growth **77**, 380 (1986).

[3] Y. Ohba, M. Ishikawa, H. Sugawara, M. Yamamoto, and T. Nakanisi, J. Cryst. Growth **77**, 374 (1986).

[4] M. Kondow and S. Minagawa, J. Appl. Phys. **64**, 793 (1988).

[5] C. Nozaki, Y. Ohba, H. Sugawara, S. Yamasuami, and T. Nakanisi, J. Cryst. Growth **93**, 406 (1988).

[6] T. Hayakawa, K. Takahashi, K. Sasaki, M. Hosoda, S. Yamamoto, and T. Hijikata, Jpn. J. Appl. Phys. **27**, L968 (1988).

[7] C. Nozaki *et al.*, J. Cryst. Growth **93**, 406 (1988).

[8] M. Kondow, H. Kakibayashi, S. Minagawa, Y. Inoue, T. Nishino, and Y. Hamakawa, J. Cryst. Growth **93**, 412 (1988).

[9] K. Sugiura, K. Domen, M. Sugawara, C. Anayama, M. Kondo, T. Tanahashi, and K. Nakajima, J. Appl. Phys. **70**, 4946 (1991); S. Naritsuka, Y. Nishikawa, H. Sugawara, M. Ishikawa, and Y. Kokubun, J. Electron. Mater. **9**, 687 (1991).

[10] R. P. Schneider, Jr., R. P. Bryan, J. A. Lott, E. D. Jones, and G. R. Olbright, J. Cryst. Growth **124**, 763 (1992).

[11] D. J. Mowbray, O. P. Kowalski, M. Hopkinson, M. S. Skolnick, and J. P. R. David, Appl. Phys. Lett. **65**, 213 (1994); M. Hopkinson, J. P. R. David, O. P. Kowalski, D. J. Mowbray, and M. S. Skolnick, *Proceedings of Sixth International Conference on Indium Phosphide and Related Materials* (IEEE, New York, 1994), pp. 567–570.

[12] A. D. Prins, J. L. Sly, A. T. Meney, D. J. Dunstan, E. O'Reilly, A. R. Adams, and A. Valster, in *Proceedings of the 22nd International Conference on the Physics of Semiconductors*, edited by D. J. Lockwood (World Scientific, Singapore, 1995), pp. 727–730.

[13] P. Gavrilovic, F. P. Dabkowski, K. Meehan, J. E. Williams, S. Stutius, K. C. Hseih, N. Holonyak, Jr., M. A. Shahid, and S. Mahajan, J. Cryst. Growth **93**, 426 (1988).

[14] Y. Hamisch, R. Steffen, A. Forchel, and P. Rontgen, Appl. Phys. Lett. **62**, 3007 (1993).

[15] A. Ishibashi, M. Mannoh, I. Kidoguchi, Y. Ban, and K. Ohnaka, Appl. Phys. Lett. **65**, 1275 (1994).

[16] V. Swaminatchan and A. T. Macrander, *Material Aspects of GaAs and InP Based Structures* (Prentice-Hall, Englewood Cliffs, NJ, 1991).

[17] W.-K. Chu, J. W. Mayer, and M.-A. Nicolet, *Backscattering Spectrometry* (Academic, New York, 1978); J. F. Ziegler, *Helium Stopping Powers and Ranges in All Elemental Matter* (Pergamon, New York, 1977); S. R. Lee and R. R. Hart, Nucl. Instrum. Methods B **79**, 463 (1993); H. H. Anderson, F. Besenbacher, P. Loftager, and W. Moller, Phys. Rev. B **21**, 1891 (1980).

[18] H. Ackerman, E. D. Jones, J. E. Schirber, and D. L. Overmyer, Cryogenics **25**, 496 (1985).

[19] D. M. Follstaedt, R. P. Schneider, Jr., and E. D. Jones, J. Appl. Phys. **77**, 3077 (1995).

[20] M. Schluter, J. R. Chelikowsky, S. G. Louie, and M. L. Cohen, Phys. Rev. B **12**, 4200 (1975); J. Ihm, A. Zunger, and M. L. Cohen, J. Phys. C **12**, 4409 (1979); K. C. Pandey, Phys. Rev. Lett. **49**, 223 (1982); W. E. Pickett, Comput. Phys. Rep. **9**, 115 (1989); G. P. Srivastava and D. Weaire, Adv. Phys. **36**, 463 (1987).

[21] E. D. Jones and G. L. Wickstrom, SPIE **540**, 362 (1985).
[22] E. D. Jones, I. J. Fritz, H. P. Hjalmarson, J. E. Schirber, M. C. Smith, R. M. Biefeld, L. R. Dawson, and T. J. Drummond, SPIE **792**, 117 (1987).
[23] S. Wei, L. G. Ferreira, J. E. Bernard, and A. Zunger, Phys. Rev. B **42**, 9622 (1990).
[24] D. M. Ceperley and B. J. Alder, Phys. Rev. Lett. **45**, 566 (1980); see parametrization by J. Perdew and A. Zunger, Phys. Rev. B **23**, 5048 (1981).
[25] P. Hohenberg and W. Kohn, Phys. Rev. **136**, B864 (1964); see also W. Kohn and L. J. Sham, *ibid.* **140**, A1133 (1965); in addition, see *Theory of the Inhomogeneous Electron Gas,* edited by S. Lundqvist and N. M. March (Plenum, New York, 1983).
[26] D. R. Hamann, Phys. Rev. B **40**, 2980 (1989).
[27] S. G. Louie, S. Froyen, and M. L. Cohen, Phys. Rev. B **26**, 1738 (1982).
[28] H. J. Monkhorst and J. D. Pack, Phys. Rev. B **13**, 5188 (1976).
[29] S. Froyen, Phys. Rev. B **39**, 3168 (1989).
[30] M. C. Delong, D. J. Mowbray, R. A. Hogg, M. S. Skolnick, J. E. Williams, K. Meehan, S. R. Kurtz, J. M. Olsen, R. P. Schneider, M. C. Wu, and M. Hopkinson, Appl. Phys. Lett. **66**, 3185 (1995).
[31] A. F. Wright and J. S. Nelson, Phys. Rev. B **52**, 1011 (1995).
[32] O. Madelung, *Semiconductors Group IV Elements and III-V Compounds* (Springer-Verlag, New York, 1987).
[33] X. Zhu and S. G. Louie, Phys. Rev. B **43**, 14 142 (1993).